Combustion and Flame 281 (2025) 114396

Contents lists available at ScienceDirect

Combustion and Flame

journal homepage: www.sciencedirect.com/journal/combustion-and-flame

Flame dynamics of nonpremixed coflow DME jets in momentum-driven and buoyancy-momentum-driven regimes

Dong Jun Kim [a], Jeong Park [b,*], Suk Ho Chung [c], Chun Sang Yoo [a,*]

[a] Department of Mechanical Engineering, Ulsan National Institute of Science and Technology, Ulsan, Republic of Korea
[b] Department of Mechanical Engineering, Pukyong National University, Busan, Republic of Korea
[c] Clean Combustion Research Center (CCRC), King Abdullah University of Science and Technology, Thuwal, Saudi Arabia

ARTICLE INFO

Keywords:
Laminar nonpremixed flames
Dimethyl ether (DME)
Richardson number
Liftoff height
Buoyancy and jet momentum interaction

ABSTRACT

This study experimentally investigates the behavior of laminar nonpremixed flames of N_2-diluted Dimethyl ether (DME) in a coflow jet under varying fuel mole fractions ($X_{F,0}$), jet velocities (U_0), and temperatures (T_0 = 300, 400, and 500 K). A wide range of lifted flame behaviors is observed as U_0 increases, including three distinct trends in liftoff height (H_L): Monotonically increasing (M.I.), Monotonically decreasing (M.D.), and U-shaped H_L. In addition, two flame extinction modes (i.e., flame blowoff and blowout) are identified depending on the jet developing length (Z_{free}). The observed flame behaviors are classified into three different regimes based on the Richardson number (Ri): Momentum-driven (MD), Buoyancy-momentum-driven (BMD), and Buoyancy-driven (BD) regimes. The monotonically decreasing H_L behavior appears exclusively in the buoyancy-momentum-driven regime, where buoyancy effects remain significant. In contrast, the monotonically increasing H_L behavior is confined to the momentum-driven regime, where jet momentum dominates. The U-shaped H_L behavior emerges during the transition between the buoyancy-momentum-driven and momentum-driven regimes. To elucidate the underlying stabilization mechanisms, time-resolved flame edge measurements are conducted using laser ignition downstream of the nozzle, from which flame stabilization and blowout mechanisms are identified for each regime. In the buoyancy-momentum-driven regime, flame liftoff is influenced by a combination of buoyancy, jet momentum, and heat loss to the nozzle rim. In the momentum-driven regime, jet momentum is the dominant factor. Correlations for H_L are developed in terms of the laminar flame speed (S_L^0), U_0, T_0, $X_{F,0}$, and Ri, reflecting the regime-dependent influence of buoyancy and momentum. Finally, the flame blowoff and liftoff limits of attached flames are characterized using the density difference between fuel and burnt gas, U_0/S_L^0, and a heat loss parameter, revealing the role of heat loss in flame liftoff processes. These findings provide a unified understanding of lifted flame behavior and extinction mechanisms under various flow and thermal conditions.

Novelty and significance statement

This study establishes a unified regime-based framework for lifted flame behavior by introducing three regimes: the momentum-driven (MD) regime, the buoyancy–momentum-driven (BMD) regime, and the buoyancy-driven (BD) regime, all defined based on the Richardson number. Unlike prior studies limited to specific conditions, this study explains diverse lifted flame behaviors, including U-shaped, increasing, and decreasing variations with jet velocity, across a broad range of conditions. By identifying distinct extinction modes, such as flame blowout and blowoff, and revealing the role of nozzle heat loss in the BMD regime, this study advances the understanding of flame stabilization and limit phenomena beyond previously known mechanisms.

1. Introduction

Understanding how turbulent lifted jet flames stabilize under various conditions is essential for designing stable and efficient burners and combustors. To advance this understanding, extensive research has been conducted on laminar lifted jet flames [1–6], providing valuable insights into their behavior. In a laminar fuel jet, a lifted flame exhibits a tribrachial edge structure with a rich premixed flame, a lean premixed flame, and a trailing diffusion flame extending from a tribrachial point

* Corresponding authors.
E-mail addresses: jeongpark@pknu.ac.kr (J. Park), csyoo@unist.ac.kr (C.S. Yoo).

https://doi.org/10.1016/j.combustflame.2025.114396
Received 12 April 2025; Received in revised form 5 August 2025; Accepted 5 August 2025
Available online 20 August 2025

Nomenclature

Symbols

D	Inner diameter of the nozzle
H_L	Liftoff height
H_e	Flame edge height
R	Correlation coefficient
S_L^0	Laminar flame speed
S_e	Edge flame speed
T_0	Initial temperature
T_{ad}	Adiabatic temperature
T_f	Flame temperature
T_{ref}	Reference temperature
U_0	Initial jet velocity
U_b	Baseline velocity
V_L	Local flow velocity
V_{co}	Coflow air velocity
$X_{F,0}$	Initial fuel mole fraction
Z_{free}	Jet developing length
ρ_F	Fuel gas density
ρ_b	Burnt gas density
Re_D	Reynolds number
Ri	Richardson number
Sc_F	Fuel Schmidt number
g	Gravitational acceleration

Abbreviations

BD	Buoyancy-driven
BMD	Buoyancy-momentum-driven
DME	Dimethyl ether
M.D.	Monotonically decreasing
M.I.	Monotonically increasing
MD	Momentum-driven

along the stoichiometric contour. A theoretical study revealed that for pure fuel jet issuing from a sub-millimeter nozzle, the lifted flame can stabilize at the tribrachial point where the edge flame speed (S_e) balances local flow velocity (V_L) [1]. For pure fuels with Schmidt number (Sc_F) larger than unity, such as propane and butane, stable lifted flames in free jets were observed, whereas for fuels with $Sc_F < 1$, such as methane and ethylene, lifted jet flames did not exist [1,2].

The stabilization of the laminar lifted jet flame is attributed to the balance between S_e and V_L. However, both S_e and V_L are governed by several factors: S_e is influenced by flow redirection, mixture strength, fuel concentration gradient, strain rate, flame curvature, Lewis number, and other parameters [7–10], while V_L is primarily determined by the fuel jet velocity (U_0). When U_0 is too low, however, buoyancy can significantly affect V_L by entraining surrounding air [11–17]. For methane/nitrogen jets issuing from relatively large nozzles, the behavior of the lifted jet flame has been observed to vary significantly due to the influence of buoyancy [12].

Recent studies on methane and ethylene coflow jets diluted with helium, nitrogen, and argon, with Sc_F ranging from 0.70 to 1.34, revealed a unique pattern in the liftoff height (H_L) of lifted flames, wherein H_L initially decreased and then increased with increasing U_0 [13,16]. It was first hypothesized that the observed trend might be associated with Sc_F values less than unity. To further examine the effect of Sc_F, we subsequently investigated nitrogen-diluted dimethyl ether (DME) jets with $Sc_F > 1.0$ [17]. These experiments showed that H_L increased as U_0 decreased, ultimately leading to flame blowout at relatively low jet velocities. This was attributed to the dominance of buoyancy over jet momentum in determining the local velocity V_L near the stabilization point, rather than to the effect of Sc_F.

DME fuel has a relatively low autoignition temperature of 623 K compared to other hydrocarbon fuels and is known for its low particulate emissions and high cetane number, making it an environmentally friendly fuel widely studied for automotive engine applications. Consequently, numerous studies have explored the behavior and structure of DME lifted jet flames at temperatures exceeding its autoignition point [18–20]. Additionally, under conditions where DME is highly diluted with nitrogen at temperatures above its autoignition point, numerical simulations have revealed a decreasing trend in H_L with increasing U_0 at relatively low velocities. This behavior was attributed to differential diffusion effects caused by DME pyrolysis [19].

Building on the aforementioned investigations, this study investigates the behavior of laminar nonpremixed flames of N_2-diluted DME jets under various conditions. The temperature (T_0) of the coflow air varies between 300 and 500 K, while nitrogen dilution and U_0 are adjusted, all under conditions where $Sc_F > 1.0$. Three distinct flame behaviors are identified: monotonically increasing (M.I.) H_L, U-shaped H_L, and monotonically decreasing (M.D.) H_L. Flame extinction modes are classified into two categories based on the jet developing length (Z_{free}): flame blowout and flame blowoff. Flame blowout refers to the extinction of a lifted flame in the fully developed region, whereas flame blowoff denotes extinction in the developing region without noticeable flame liftoff. Furthermore, the lifted flame behaviors are categorized into momentum-driven (MD), buoyancy-momentum-driven (BMD), and buoyancy-driven (BD) regimes. To further identify the stabilization mechanisms of lifted flames in these regimes, their propagation processes are analyzed by initiating the flame using a laser. Finally, H_L and the limits of flame blowout and blowoff are characterized in terms of their associated physical parameters, providing deeper insights into the stabilization and extinction dynamics of DME jet flames.

2. Experimental setup

The apparatus consisted of a coflow burner, a flow control system, a heating system, and a visualization setup, as schematically shown in Fig. 1. The coflow burner is composed of a fuel jet and an air coflow section, both housed in a cylindrical structure. The jet is positioned at the center of the coflow, with an inner diameter (D) of 4 mm, an outer diameter of 6 mm, and a length of 600 mm, ensuring a fully developed flow. The coflow section has a diameter of 93 mm and contains metal fiber, ceramic beads, and a ceramic honeycomb to ensure uniform coflow and maintain uniform temperature. The nozzle tip protrudes 10 mm above the coflow exit.

Flow rates are controlled using mass flow controllers. DME (> 99.99% purity) is used as fuel, diluted with N_2 (> 99.999% purity), while compressed air serves as oxidizer. The heating system employs four coil heaters (4.4 kW) to preheat the air. Ceramic screens inside the burner act as a thermal reservoir to minimize temperature fluctuations. A type-K thermocouple (1.0 mm) is used to measure the radial temperature of the heated air, ensuring all experiments are conducted within a ±5 K deviation in the radial temperature profile at the air outlet.

Flame images are captured using a DSLR camera, and H_L is defined as the distance from the nozzle to the flame edge, determined via image processing with a MATLAB-based code [13–17]. Downstream ignition is initiated using an Nd:YAG laser with a maximum energy output of 1580 mJ and a spot size of 9 mm. High-speed images are captured at 200 fps using a high-speed camera.

The experimental conditions include fuel mole fraction ($X_{F,0}$) in the fuel jet ranging from 0.11 to 0.40, air temperature (T_0) of 300, 400, and 500 K, fuel jet velocity (U_0) of up to 3.50 m/s, and fixed coflow air velocity (V_{co}) of 0.30 m/s. The corresponding Reynolds number (Re_D), based on D and U_0, ranges from 13 to 983. Sc_F varies between 1.09 and 1.17.

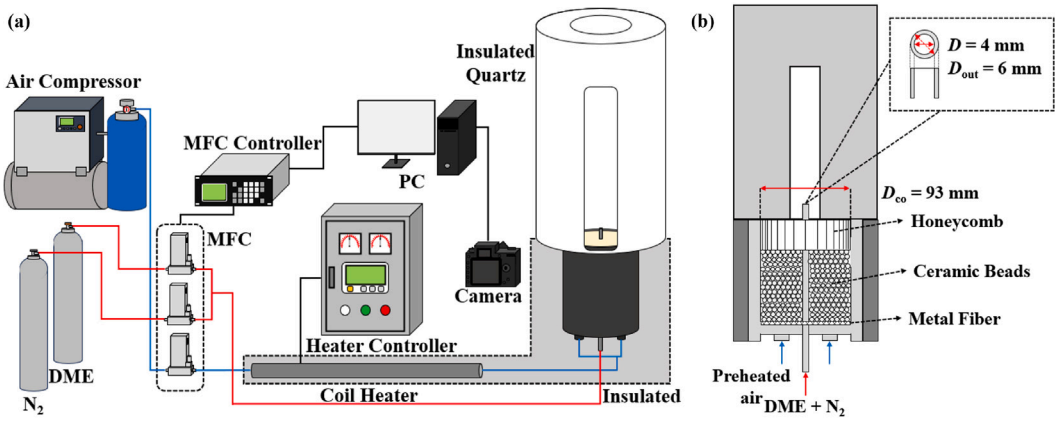

Fig. 1. Schematics of the experimental setup and coflow burner.

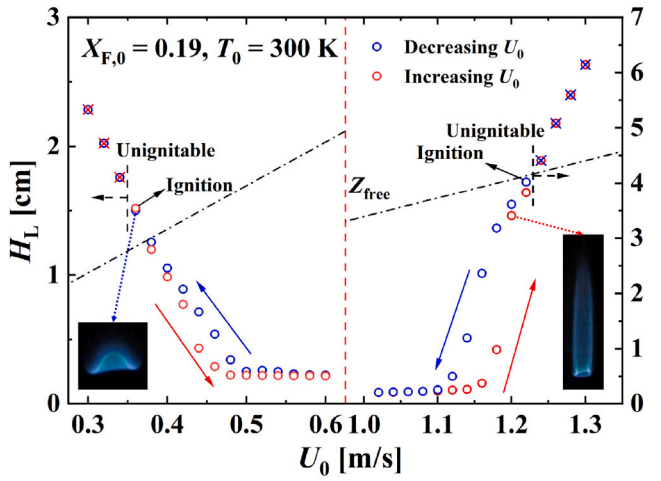

Fig. 2. Flame behaviors with increasing and decreasing jet velocity for $X_{F,0} = 0.19$ and $T_0 = 300$ K.

3. Overall flame features

Fig. 2 shows the variation in H_L as a function of U_0 when U_0 is gradually decreased and then increased at $X_{F,0} = 0.19$ and $T_0 = 300$ K, starting from an ignitable point using a torch. The direct images of two representative lifted flames at relatively high and low U_0 are also shown in the figure. It is readily observed from the direct flame images that the lifted flames exhibit a typical tribrachial edge structure, comprising a rich premixed flame, a lean premixed flame, and a trailing diffusion flame. This observation confirms the validity of applying the balance mechanism between S_e and V_L for lifted flame stabilization to the present cases as in many previous studies [1–5,11–17].

As shown in Fig. 2, in the decreasing U_0 scenario, the flame fails to ignite at $U_0 \geq 1.24$ m/s but successfully ignites at $U_0 = 1.22$ m/s, subsequently attaching to the nozzle as U_0 decreases. With further decreases in U_0, the flame eventually lifts off again and is extinguished below $U_0 = 0.3$ m/s. Similarly, in the increasing U_0 scenario, ignition does not occur at $U_0 \leq 0.34$ m/s but the flame successfully ignites at $U_0 = 0.36$ m/s, subsequently attaching to the nozzle as U_0 increases. At higher U_0, the flame lifts off again and is extinguished above $U_0 = 1.3$ m/s.

These results suggest that at relatively low U_0, the flame exhibits minimal hysteresis due to the reduced edge flame speed (S_e) caused by high N_2 dilution and the corresponding increase in quenching distance. In contrast, a clear hysteresis behavior is evident at higher U_0, similar to that observed with hydrocarbon fuels [21,22]. Although there exists the hysteresis behavior in H_L, its effect on the overall trend of H_L in response to U_0 is marginal. Therefore, experiments were conducted by varying U_0 from a baseline velocity (U_b) of 1.0 m/s to investigate a wider flammability range and obtain more comprehensive data on flame behaviors. In all cases, once a flame is ignited at $U_0 = 1.0$ m/s, the response of H_L to changes in U_0 is monitored by either increasing U_0 above 1.0 m/s or decreasing it below 1.0 m/s.

Fig. 3 shows representative direct images illustrating the behaviors of laminar nonpremixed flames of N_2-diluted DME jets in response to U_0 for various $X_{F,0}$ at $T_0 = 500$ K. It is readily observed that at $X_{F,0} = 0.11$ (Fig. 3a), H_L shows a monotonic trend with U_0; it increases with increasing U_0 above 1.0 m/s and decreases with decreasing U_0 below 1.0 m/s. At $X_{F,0} = 0.12$ (Fig. 3b), however, H_L exhibits a non-monotonic (U–shaped) response with increasing U_0. At $X_{F,0} = 0.14$ (Fig. 3c), the flame initially attaches to the nozzle at $U_0 = 1.0$ m/s, and then lifts off as U_0 increases or decreases. In this case, H_L continues to increase with either increasing or decreasing U_0 beyond 1.0 m/s, up to the point of flame blowout. At $X_{F,0} = 0.25$ (Fig. 3d), the flame remains attached to the nozzle within a range of U_0 values; beyond the extinction limits ($U_0 > 4.0$ m/s or $U_0 < 0.18$ m/s), any further increase or decrease in U_0 results in flame blowoff.

To further elucidate the flame behaviors, the variations in H_L as a function of U_0 over wide ranges of fuel content ($0.11 \leq X_{F,0} \leq 0.40$) and temperature ($T_0 = 300$, 400, and 500 K) are shown in Fig. 4. To quantify the buoyancy effect on flame stabilization, the Richardson number (Ri), defined as the ratio of buoyancy to jet momentum, is also presented. Here, Ri is calculated as $\mathrm{Ri} = (\rho_F - \rho_b)gD/\rho_F U_0^2$, where ρ_F and ρ_b represent the fuel and burnt gas densities under stoichiometric conditions, respectively. The detailed values of Ri for the flames shown in Figs. 3 and 4 are listed in Tables 1 and 2, respectively.

In addition, the jet developing length (Z_{free}), derived from free jet theory as $Z_{free}/D = 0.0165 \cdot \mathrm{Re_D}$ [11], is indicated to differentiate two distinct flame extinction modes: flame blowout and flame blowoff. In this study, flame blowout is defined as the extinction of a flame in the developed region after it has lifted off, whereas flame blowoff denotes to the extinction of a flame occurring in the developing region regardless of its liftoff. Typically, H_L preceding flame blowoff is minimal, comparable to the quenching distance, causing the flame appear as though it blows off directly without noticeable liftoff. Since the present coflow jets inherently involve a non-zero coflow velocity, their Z_{free} values are slightly different from those of free jets [11] (see Supplementary Material 1 (SM1)). However, the differences are not significant and thus, Z_{free} for free jets can be effectively used to distinguish between the two extinction modes.

In Fig. 4a, for $T_0 = 300$ K, flame blowoff occurs at relatively high $X_{F,0}$, while flame blowout is observed solely at relatively low $X_{F,0}$ for both low and high U_0. As U_0 increases from 1.0 m/s, a flame with low $X_{F,0}$ (e.g., $X_{F,0} = 0.19$) is not strong enough to remain attached to the

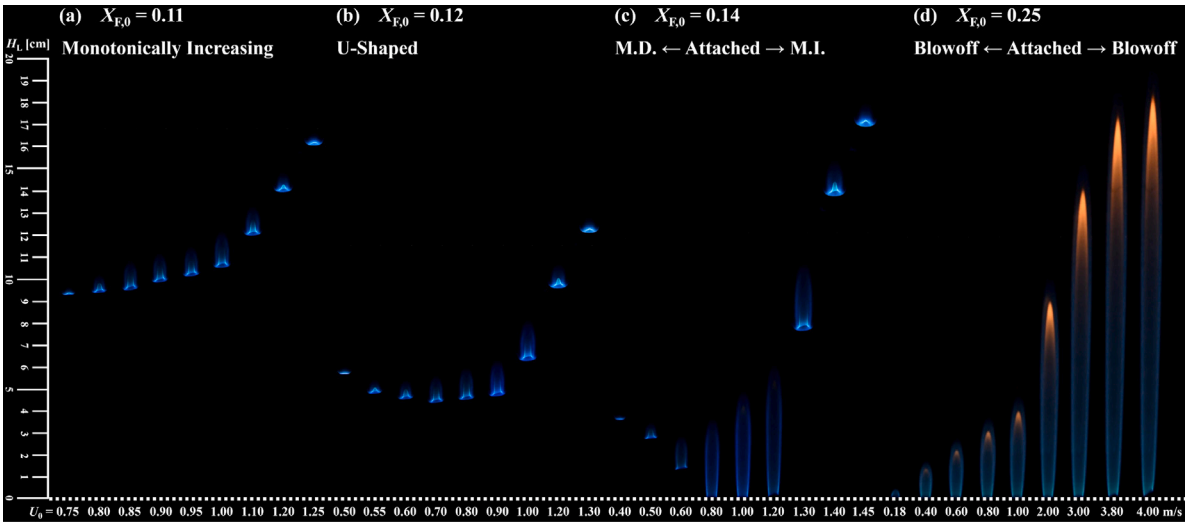

Fig. 3. Direct images of laminar nonpremixed flames of N_2-diluted DME jets in the coflow jet with V_{co} = 0.30 m/s with increasing and decreasing U_0 for (a) $X_{F,0}$ = 0.11, (b) 0.12, (c) 0.14, and (d) 0.25 at T_0 = 500 K. M.I. and M.D. represent monotonically increasing and monotonically decreasing H_L, respectively.

Table 1
Richardson numbers for laminar nonpremixed flames of N_2-diluted DME jets in the coflow jet with V_{co} = 0.30 m/s for different $X_{F,0}$ at T_0 = 500 K (see Fig. 3).

$X_{F,0}$ = 0.11		$X_{F,0}$ = 0.12		$X_{F,0}$ = 0.14		$X_{F,0}$ = 0.25	
U_0 [m/s]	Ri	U_0 [m/s]	Ri	U_0 [m/s]	Ri	U_0 [m/s]	Ri
0.75	0.0531	0.50	0.1201	0.40	0.1894	0.18	0.9577
0.80	0.0467	0.55	0.0993	0.50	0.1212	0.40	0.1939
0.90	0.0369	0.60	0.0834	0.60	0.0842	0.60	0.0862
0.95	0.0331	0.70	0.0613	0.80	0.0474	0.80	0.0485
1.00	0.0299	0.80	0.0469	1.00	0.0303	1.00	0.0310
1.10	0.0247	0.90	0.0371	1.20	0.0210	2.00	0.0078
1.20	0.0207	1.00	0.0300	1.30	0.0179	3.00	0.0034
1.25	0.0191	1.20	0.0209	1.40	0.0155	3.80	0.0021
		1.30	0.0178	1.45	0.0144	4.00	0.0019

nozzle. Consequently, the flame lifts off and then blows out at much lower U_0 compared to that with high $X_{F,0}$ (e.g., $X_{F,0}$ = 0.24). Likewise, as U_0 decreases from 1.0 m/s, a flame with low $X_{F,0}$ (e.g., $X_{F,0}$ = 0.24) lifts off and then blows out at higher U_0 compared to that with high $X_{F,0}$ (e.g., $X_{F,0}$ = 0.38). Moreover, as T_0 increases from 300 to 400 to 500 K, flame blowoff occurs at much lower $X_{F,0}$ for both low and high U_0, while Z_{free} simultaneously decreases. This flame blowoff behavior is primarily attributed to enhanced flame strength to withstand heat loss to the nozzle rim and remain anchored to the nozzle with increasing T_0. At low U_0, most of the flame extinctions in Fig. 4 occur at 0.95 < Ri < 2.36, implying that both jet momentum and buoyancy contribute to determining flame stability. These flame features will be further discussed later.

Using the data from Fig. 4 together with additional data in the range of 0.11 ≤ $X_{F,0}$ ≤ 0.40, flame stability maps in the $X_{F,0} - U_0$ space are generated for different T_0, as shown in Fig. 5. As discussed above, flame extinction occurs through either flame blowout or blowoff. Moreover, three distinct H_L behaviors are observed at relatively low $X_{F,0}$ and U_0. As mentioned above, the experiments were conducted by either increasing or decreasing U_0 from the baseline velocity (U_b = 1.0 m/s), as indicated by the dashed lines and arrows in the figure.

It is also readily observed that, for all cases, an increase in T_0 strengthens the flame, leading to a reduction in the regions of both flame blowout and blowoff with the corresponding boundaries shifting toward lower $X_{F,0}$. Similarly, for all lifted flames with three distinct H_L behaviors, their corresponding regions shrink and shift toward lower $X_{F,0}$ as T_0 increases. Consequently, the region of attached flames expands toward lower $X_{F,0}$ with increasing T_0. This is also primarily attributed to the increase in flame strength, represented by flame temperature (T_f). Note that the adiabatic flame temperatures (T_{ad}) of a stoichiometric DME/air mixture with $X_{F,0}$ = 0.19 are approximately 2031, 2091, and 2150 K at T_0 = 300, 400, and 500 K, respectively [23]. Note that the adiabatic flame temperatures values were evaluated using the PREMIXED code [24] with a detailed kinetic mechanism for DME oxidation [25]. This confirms the flame strength is enhanced with increasing T_0.

4. Lifted flame characteristics

4.1. Flame regime classification and H_L characteristics

As shown in Figs. 3–5, the lifted flames exhibit three distinct H_L behaviors, which appear to be significantly related to the balance between the buoyancy and jet momentum, or Ri. To better describe these observations, the flames are categorized into three different regimes based on Ri, analogous to thermal convection problems involving both forced and natural convections. Typically, forced convection is dominant over natural convection when Ri < 0.1, whereas natural convection predominates when Ri > 10. Both convection modes significantly influence the flow in the intermediate range (0.1 < Ri < 10).

Accordingly, flame behaviors are classified into three distinct regimes: (1) the momentum-driven (MD) regime for Ri < 0.1, (2) the buoyancy-momentum-driven (BMD) regime for 0.1 < Ri < 10, and (3) the buoyancy-driven (BD) regime for Ri > 10. The MD regime corresponds to conditions in which jet momentum strongly dominates over buoyancy, while the BD regime represents conditions dominated by buoyancy forces. Meanwhile, the BMD regime encompasses transitional conditions in which both jet momentum and buoyancy substantially

Table 2
Richardson numbers for laminar nonpremixed flames of N_2-diluted DME jets in the coflow jet with $V_{co} = 0.30$ m/s for different $X_{F,0}$ at $T_0 = 300$, 400, and 500 K (see Fig. 4.)

$T_0 = 300$ K								
Low U_0			Intermediate U_0			High U_0		
$X_{F,0}$	U_0 [m/s]	Ri	$X_{F,0}$	U_0 [m/s]	Ri	$X_{F,0}$	U_0 [m/s]	Ri
0.24	0.19~0.35	0.9396~0.2769	0.12	0.68~1.45	0.7219~0.1588	0.19	1.00~1.75	0.0339~0.0111
0.26	0.18~0.35	1.0496~0.2776	0.14	0.48~1.55	1.4578~0.1398	0.20	1.00~1.75	0.0340~0.0111
0.28	0.17~0.35	1.1793~0.2783	0.16	0.38~1.65	2.3366~0.1239	0.21	1.00~1.80	0.0340~0.0105
0.30	0.16~0.35	1.3282~0.2784	0.17	0.34~1.70	2.9243~0.1170	0.22	1.00~1.85	0.0340~0.0099
0.32	0.15~0.35	1.5154~0.2785				0.23	1.00~1.90	0.0341~0.0094
0.34	0.14~0.35	1.7376~0.2786				0.24	1.00~1.95	0.0341~0.0090
0.36	0.135~0.35	1.8700~0.2789				0.25	1.00~2.00	0.0341~0.0085
0.38	0.13~0.35	2.0178~0.2791						
0.40	0.125~0.35	2.1837~0.2793						
$T_0 = 400$ K								
Low U_0			Intermediate U_0			High U_0		
$X_{F,0}$	U_0 [m/s]	Ri	$X_{F,0}$	U_0 [m/s]	Ri	$X_{F,0}$	U_0 [m/s]	Ri
0.24	0.19~0.35	0.8957~0.2640	0.12	0.66~1.25	0.7269~0.2027	0.19	1.00~1.95	0.0323~0.0085
0.26	0.17~0.35	1.1185~0.2646	0.14	0.44~1.50	1.6483~0.1418	0.20	1.00~2.00	0.0323~0.0081
0.28	0.16~0.35	1.2646~0.2651	0.16	0.36~1.75	2.4760~0.1048	0.21	1.00~2.05	0.0324~0.0077
0.30	0.16~0.35	1.2663~0.2655	0.17	0.32~1.85	3.1407~0.0940	0.22	1.00~2.10	0.0324~0.0074
0.32	0.15~0.35	1.4424~0.2658				0.23	1.00~2.40	0.0325~0.0056
0.34	0.14~0.35	1.6575~0.2661				0.24	1.00~2.60	0.0325~0.0048
0.36	0.14~0.35	1.6589~0.2664				0.25	1.00~3.05	0.0325~0.0035
0.38	0.13~0.35	1.9254~0.2666						
0.40	0.12~0.35	2.2612~0.2669						
$T_0 = 500$ K								
Low U_0			Intermediate U_0			High U_0		
$X_{F,0}$	U_0 [m/s]	Ri	$X_{F,0}$	U_0 [m/s]	Ri	$X_{F,0}$	U_0 [m/s]	Ri
0.24	0.18~0.35	0.9485~0.2518	0.11	0.76~1.25	0.5170~0.1911	0.19	1.00~2.25	0.0307~0.0061
0.26	0.17~0.35	1.0657~0.2524	0.12	0.54~1.40	1.0300~0.1532	0.20	1.00~2.45	0.0308~0.0051
0.28	0.16~0.35	1.2052~0.2529	0.14	0.40~1.45	1.8944~0.1442	0.21	1.00~2.75	0.0309~0.0041
0.30	0.15~0.35	1.3734~0.2534	0.16	0.32~1.85	2.9730~0.0890	0.22	1.00~3.20	0.0309~0.0030
0.32	0.14~0.35	1.5787~0.2538	0.17	0.30~1.95	3.3998~0.0805	0.23	1.00~3.50	0.0310~0.0025
0.34	0.14~0.35	1.5805~0.2541				0.24	1.00~4.05	0.0310~0.0019
0.36	0.13~0.35	1.8348~0.2544				0.25	1.00~4.55	0.0310~0.0015
0.38	0.13~0.35	1.8364~0.2546						
0.40	0.12~0.35	2.1570~0.2550						

influence flame dynamics. Within this context, the monotonically increasing H_L behavior is observed only in the MD regime, consistent with typical lifted flames in previous studies [1–6], whereas the monotonically decreasing H_L behavior is confined to the BMD regime. Consequently, the U-shaped H_L behavior emerges only when a flame transitions from the BMD to the MD regime.

For instance, all lifted flames with $X_{F,0} = 0.11$ in Fig. 3a exhibit a monotonically increasing H_L behavior and fall within the MD regime, where Ri decreases from 0.053 to 0.019 as U_0 increases from 0.75 to 1.25 m/s. In contrast, the lifted flames with $X_{F,0} = 0.14$ in Fig. 3c show a monotonically decreasing H_L behavior and fall within the BMD regime, where Ri varies from 0.189 to 0.084 as U_0 increases from 0.40 to 0.60 m/s. Meanwhile, the regime of the lifted flame with $X_{F,0} = 0.12$ in Fig. 3b transitions from the BMD to the MD regime, with Ri decreasing from 0.12 to 0.018 as U_0 increases from 0.5 to 1.3 m/s. Consequently, H_L exhibits a decreasing trend at lower U_0 values with relatively large Ri (> 0.1) and an increasing trend at higher U_0 values with relatively small Ri (< 0.1), consequently leading to a U-shaped behavior in H_L across the entire range of U_0.

It is important to note that flames in the BD regime were not observed in this study, primarily due to the limited nozzle diameter ($D = 4$ mm). It is noteworthy that Delichatsios [26] investigated flame height variations in both laminar and turbulent regimes for attached flames, while Wen et al. [27] examined the non-dimensional flame height behaviors in both attached and lifted flames under transition and turbulent conditions. In both studies, the domains of buoyancy and momentum were characterized using the Froude number. However, our previous studies [13–17] have shown that density differences between fuels and burnt gases play a significant role in determining the behavior of lifted flames, particularly within the laminar regime. Therefore, to properly evaluate the relative contributions of buoyancy and momentum in this regime, it is necessary to assess the effect of density differences by comparing the order of magnitude of the Richardson number (Ri).

4.2. Characterization of H_L

Building upon the above analysis and the balance mechanism between S_e and V_L accounting for the stabilization of the lifted flames, here we characterize H_L in both MD and BMD regimes using several key parameters, expressed as: $H_L \sim f(S_L^0, X_{F,0}, T_0, U_0, \mathrm{Ri})$. Here, S_L^0 is one of the most important factors to determine S_e; $X_{F,0}$ can represent the flame strength, thereby affecting S_e; T_0 usually affects S_e by changing S_L^0; U_0 plays a dominant role in determining V_L, while Ri is adopted to account for the buoyancy effect, thereby distinguishing between the MD and BMD regimes.

In Fig. 6a, H_L in the MD regime is characterized as a function of U_0/S_L^0, T_0/T_{ref}, and $X_{F,0}$, where S_L^0 is the laminar burning velocity of a stoichiometric DME/air mixture at 1.0 atm, calculated using the PREMIXED code [24], and T_{ref} is the reference temperature of 300 K. The best fit is given by:

$$H_L/D = 0.33 \cdot (U_0/S_L^0)^{2.0}(T_0/T_{ref})^{-0.3} X_{F,0}^{-1.8} - 45.6, \quad (1)$$

with $R = 0.96$. This expression indicates that H_L increases with increasing U_0, while it decreases with increasing T_0 and $X_{F,0}$.

In summary, within the MD regime, H_L is governed by the balance between V_L, represented by U_0/S_L^0, and S_e, influenced by T_0 and $X_{F,0}$. It is also worth noting that the exponent of Ri is found to be zero in the

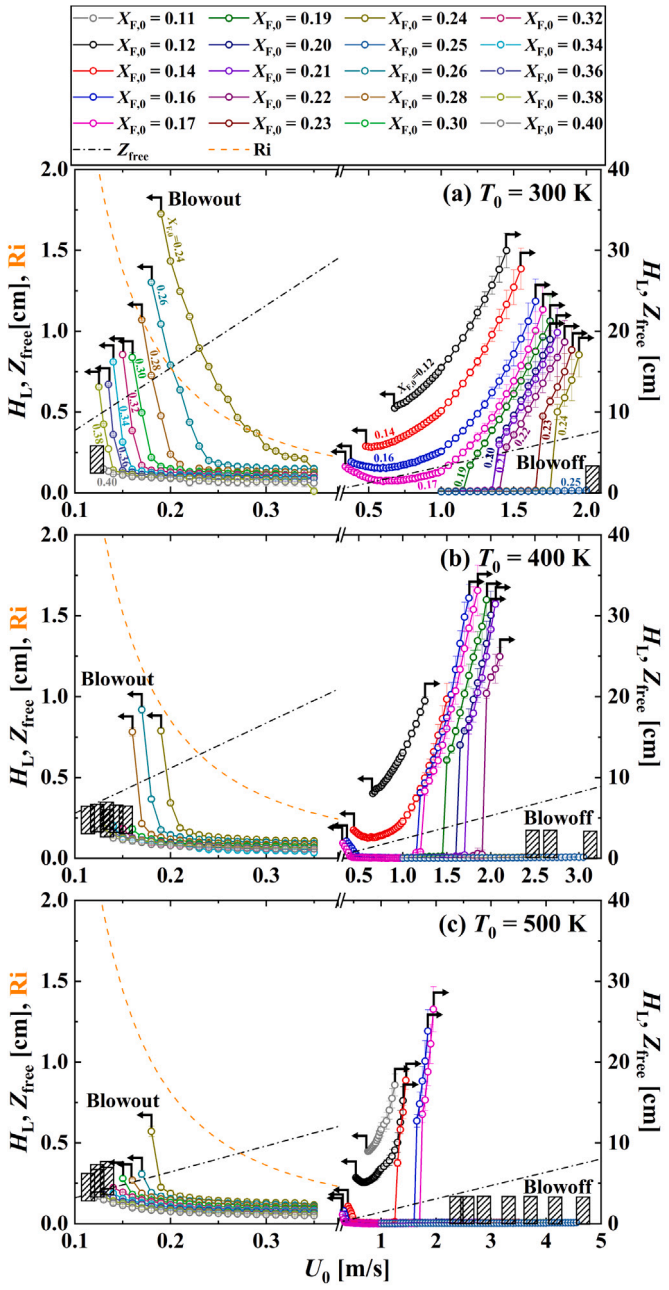

Fig. 4. Liftoff height (H_L) against fuel jet velocity (U_0) in N_2-diluted DME laminar jets at various $X_{F,0}$ for (a) T_0 = 300, (b) 400, and (c) 500 K. The dash-dotted and dashed lines represent the jet developing length (Z_{free}) and Richardson number (Ri), respectively.

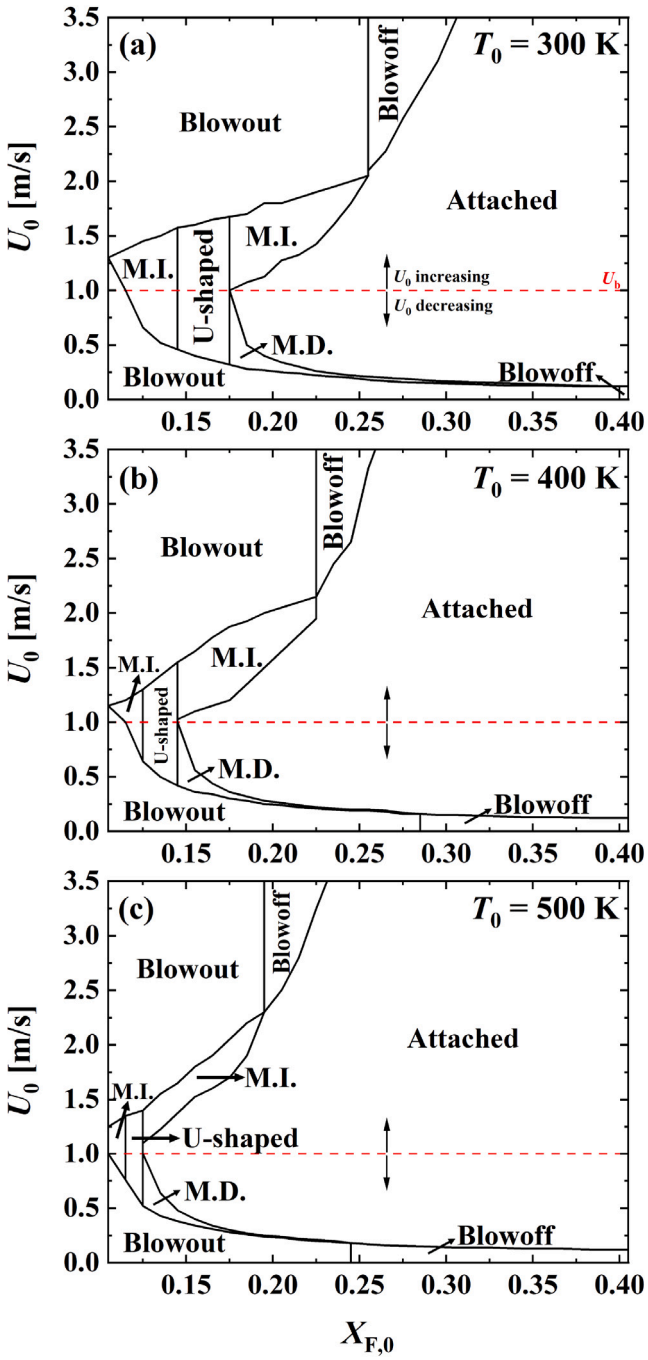

Fig. 5. Flame stability map in the U_0–$X_{F,0}$ space for (a) T_0 = 300, (b) 400, and (c) 500 K. M.I. and M.D. represent monotonically increasing and monotonically decreasing H_L, respectively.

best-fit, confirming that buoyancy has a negligible influence on H_L in the MD regime, as expected.

Fig. 6b presents the characterization of H_L in the BMD regime using Ri, T_0/T_{ref}, and $X_{F,0}$. The best fit is expressed as:

$$H_L/D = 0.81 \cdot \mathrm{Ri}^{0.6}(T_0/T_{ref})^{-0.6}X_{F,0}^{-1.8} - 6.1, \quad (2)$$

with $R = 0.91$. incorporating that H_L increases with increasing Ri, while it decreases with increasing T_0 and $X_{F,0}$. In the BMD regime, Ri is found to be a more effective parameter for characterizing H_L, indicating that buoyancy plays a critical role in determining H_L unlike in the MD regime. In summary, H_L in the BMD regime is governed by the balance between V_L, characterized through Ri, and S_e, affected by T_0/T_{ref} and $X_{F,0}$.

5. Limit phenomena

In this section, limit phenomena including flame liftoff, blowoff, and blowout are discussed to further elucidate the characteristics of laminar nonpremixed flames of N_2-diluted DME jets in the coflow jet.

5.1. Flame liftoff in the MD and BMD regimes

As shown in Fig. 3c for $X_{F,0}$ = 0.14, flame liftoff is observed in both relatively high and low U_0. At relatively high U_0 (~ 1.3 m/s), flame liftoff occurs exclusively within the MD regime with very low

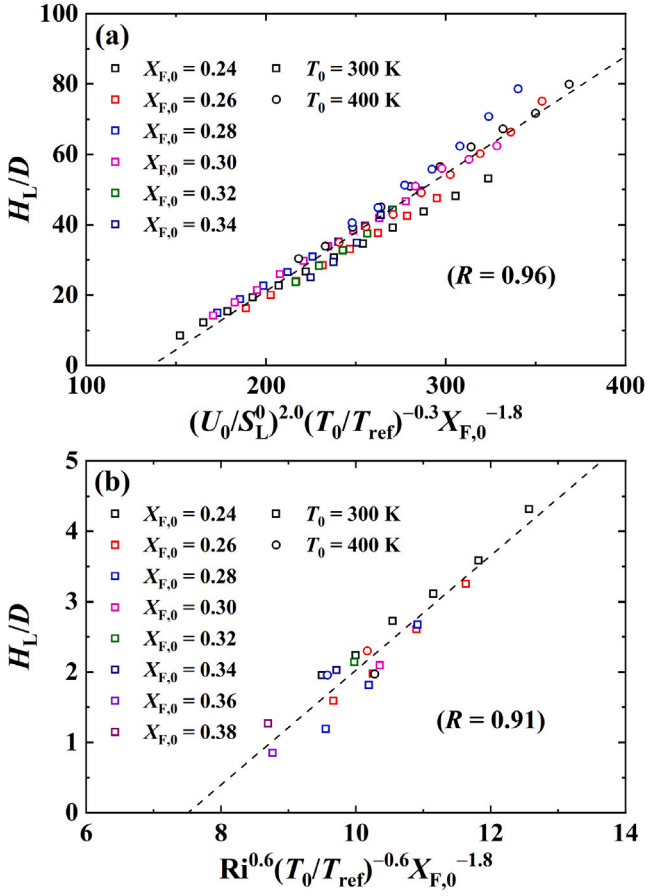

Fig. 6. Characterization of the flame liftoff height in (a) the momentum-driven (MD) regime and (b) the buoyancy-momentum-driven (BMD) regime.

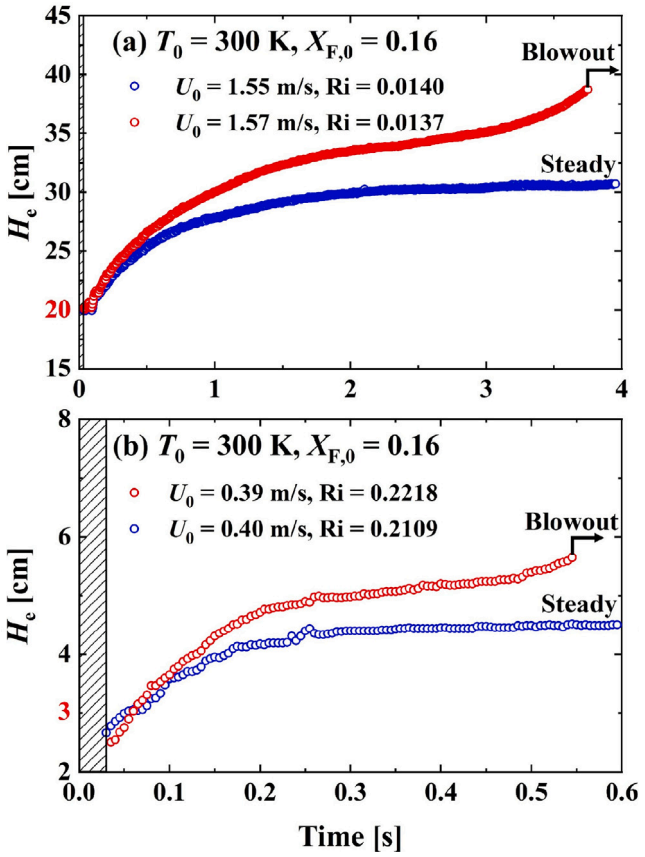

Fig. 7. Flame edge height (H_e) over time after ignition for flames in (a) the momentum-driven (MD) and (b) buoyancy-momentum-driven (BMD) regimes for $X_{F,0}$ = 0.16 at T_0 = 300 K.

Ri (~ 0.01), indicating that buoyancy has minimal influence on the liftoff process. In contrast, at relatively low U_0 (~ 0.6 m/s), flame liftoff occurs at Ri ~ 0.1 during the transition from the MD to the BMD regime, suggesting that both buoyancy and jet momentum contribute significantly to the liftoff process.

At high U_0 in the MD regime, the flame liftoff mechanism can be explained by the imbalance between the flame speed of the premixed flame segment of the nonpremixed flame and the local velocity at the flame base, as demonstrated in [28]. Similarly, at low U_0, the flame liftoff is also driven by the mismatch between the flame speed and local velocity. Specifically, in the BMD regime or during the transition from the MD to the BMD regime, the local velocity becomes increasingly influenced by buoyancy rather than jet momentum, as indicated by Ri, while the flame speed is more affected by heat loss to the nozzle. This suggests that heat loss from the flame to the nozzle rim may play a significant role in determining flame liftoff at low U_0. Note that flame liftoff occurs within the BMD regime for T_0 = 300 K, whereas it takes place during the transition from the MD to the BMD regime for T_0 = 400 or 500 K.

To qualitatively assess heat loss from the flame and better understand the liftoff process of attached flames, a previous asymptotic analysis of a premixed flame on a porous plug burner is revisited [29]. This analysis revealed that, under realistic conditions, heat loss generally decreases with increasing mass flow rate or U_0. Considering that an attached flame on the nozzle rim likely experiences similar heat loss behavior to that on a porous plug burner, it follows that heat loss in the attached flame at low U_0 can exceed that in the MD regime at high U_0. These insights suggest that, at low U_0, flame liftoff is likely driven by enhanced heat loss in combination with local velocity near the nozzle induced by both jet momentum and buoyancy. In contrast, at high U_0 in the MD regime, flame liftoff is primarily governed by jet momentum, with heat loss playing a minimal role due to its relatively lower magnitude compared to that at low U_0.

The heat loss effect on the flame liftoff needs to be further elucidated by introducing a heat loss parameter to characterize the liftoff and blowoff limits. It is worth noting that the interaction between the flame and the wall encompasses complex phenomena such as radical loss and changes in chemical kinetics as well as heat loss [30,31]. Therefore, these effects will be explored in future studies.

5.2. Flame blowout in the MD and BMD regimes

As shown in Fig. 3, flame blowout occurs in both the MD and BMD regimes. In the BMD regime, the lifted flame exhibits a monotonically increasing H_L trend with decreasing U_0, eventually leading to flame blowout. In the MD regime, however, H_L increases monotonically with increasing U_0, ultimately leading to flame blowout. The mechanisms underlying these flame stabilization and blowout processes were previously explained [17]. However, a more detailed understanding of the dynamics governing lifted flame behavior is still needed. To this end, Fig. 7 presents the temporal evolution of the flame edge height (H_e) for propagating flames in both the MD and BMD regimes. Here, H_e represents the instantaneous H_L of a propagating flame (see the SM2 for videos).

The propagating flames were initiated using a laser. Due to the high laser intensity, H_e could not be measured during the early ignition stage; this period is indicated by the hatched regions in Fig. 7. To effectively capture the flame propagating process, ignition was initiated

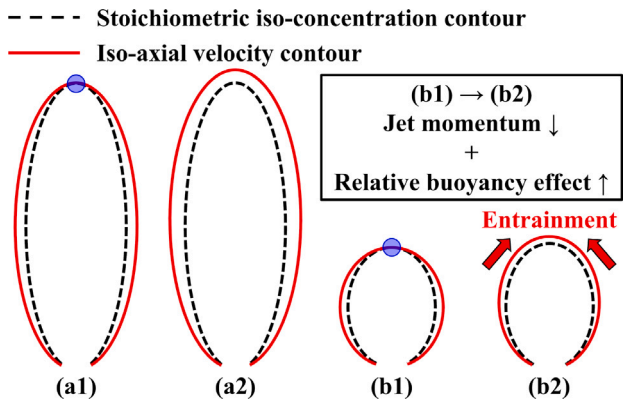

Fig. 8. Schematic of flame stabilization; a lifted flame with stable crossing when $Sc_F > 1$ (a1) and without stable crossing as U_0 increases (a2) in the momentum-driven (MD) regime; a lifted flame with stable crossing (b1) and without stable crossing as U_0 decreases (b2) in the buoyancy-momentum-driven (BMD) regime.

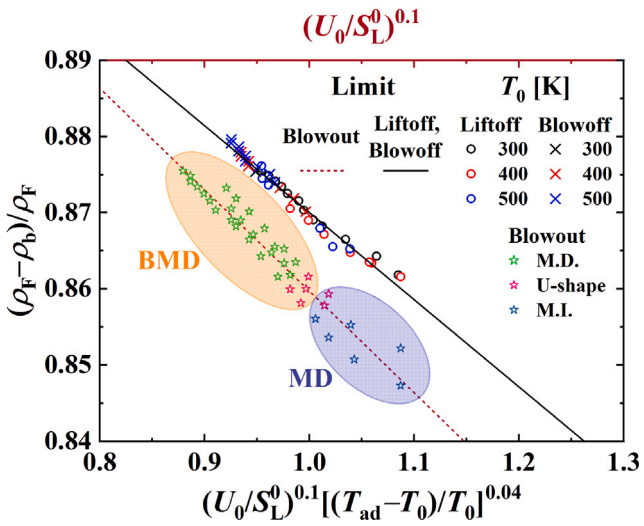

Fig. 9. Characterization of liftoff/blowoff and blowout limits. M.I. and M.D. represent monotonically increasing and monotonically decreasing H_L, respectively; BMD and MD denote the buoyancy-momentum-driven and momentum-driven regimes, respectively.

20 cm and 3 cm downstream of the nozzle for the MD and BMD regimes, respectively.

As shown in Fig. 7a, for $X_{F,0} = 0.16$ in the MD regime (Ri < 0.1), the lifted flame stabilizes at $U_0 = 1.55$ m/s (Ri = 0.0140), while it blows out at $U_0 = 1.57$ m/s (Ri = 0.0137). Since ignition is initiated upstream of the steady liftoff height at $U_0 = 1.55$ m/s, the lifted flame propagates downstream and eventually stabilizes in a nearly flat shape at steady state. This behavior implies that the iso-velocity and iso-concentration contours intersect at nearly a single point, consistent with the stabilization mechanism of lifted flames just prior to blowout [1,6]. At $U_0 = 1.57$ m/s, however, the lifted flame continues to propagate downstream, ultimately leading to blowout. This indicates that the iso-velocity contour expands both vertically and laterally compared to that at $U_0 = 1.55$ m/s, preventing it from intersecting with the iso-concentration contour, which ultimately leads to flame blowout. The mechanisms of stabilization and flame blowout for lifted flames are schematically illustrated in Figs. 8a1 and 8a2, corresponding to the stable lifted flame at $U_0 = 1.55$ m/s and the flame blowout at $U_0 = 1.57$ m/s, respectively.

Similarly, Fig. 7b shows that for $X_{F,0} = 0.16$ in the BMD regime (0.1 < Ri < 10), the lifted flame stabilizes at $U_0 = 0.40$ m/s (Ri = 0.2109), whereas it blows out at a slightly lower U_0 of 0.39 m/s (Ri = 0.2218). As ignition is initiated upstream of the steady liftoff height at $U_0 = 0.40$ m/s, the flame propagates downstream. As a result, H_e gradually increases and eventually stabilizes, forming a stable intersection between the iso-velocity and iso-concentration contours, as illustrated in Fig. 8b1. However, when U_0 decreases slightly from 0.40 to 0.39 m/s, the jet momentum weakens, while the relative influence of buoyancy increases due to the higher Ri. This causes the iso-velocity contour to elongate more than the iso-concentration contour, preventing their intersection and ultimately resulting in flame blowout, as illustrated in Fig. 8b2.

Although the intersection of the iso-velocity and iso-concentration contours is prohibited at flame blowout in both regimes, the primary mechanisms driving flame blowout differ: jet momentum dominates in the MD regime, whereas buoyancy plays a significant role in the BMD regime. These observations support the proposed mechanisms of flame stabilization and blowout in both regimes. While the study by Van et al. [13] explored the mechanism underlying the U-shaped behavior through numerical simulations conducted under conditions with Schmidt numbers less than unity, to the best of our knowledge, no prior study has addressed the influence of buoyancy on this behavior for cases where the Schmidt number exceeds unity. This study focuses on experimentally characterizing flame behaviors across various regimes and a detailed investigation of regime-specific flame characteristics using numerical simulations is planned for future work.

5.3. Characterization of liftoff, blowoff, and blowout

In our previous study [17], the flame blowout limit was successfully characterized in terms of $(\rho_F - \rho_b)/\rho_F$ and U_0/S_L^0, representing the effects of buoyancy and balance between V_L and S_e, respectively (see Fig. 9 in [17]). Building upon this analysis, the flame liftoff and blowoff limits are characterized by incorporating the heat loss effect at flame liftoff from the nozzle through a heat loss parameter represented by $(T_{ad} - T_0)/T_0$. The heat transfer from the flame to the nozzle rim is assumed to be proportional to the temperature difference between the flame and the nozzle rim, which can be approximated by T_{ad} and T_0, respectively. Accordingly, the proposed heat loss parameter serves as a simple, normalized measure of the heat loss from the flame to the nozzle rim.

Fig. 9 shows the limit for both flame blowoff and liftoff, of which best fit is given by:

$$(\rho_F - \rho_b)/\rho_F = -0.14 \cdot (U_L/S_L^0)^{0.1}[(T_{ad} - T_0)/T_0]^{0.04} + 1.0, \quad (3)$$

with $R = 0.98$, where U_L is the value of U_0 just before flame blowoff or liftoff. For comparison purposes, the flame blowout limits in this study are also shown in the figure, of which best fit is described by:

$$(\rho_F - \rho_b)/\rho_F = -0.13 \cdot (U_L/S_L^0)^{0.1} + 0.99, \quad (4)$$

with $R = 0.93$.

As shown in [17], the three lifted flame behaviors near the blowout limit are clustered according to the density difference $((\rho_F - \rho_b)/\rho_F)$ as follows: monotonically decreasing H_L in the range of 0.862–0.876, U-shaped H_L in 0.857–0.861, and monotonically increasing H_L in 0.847–0.856. In addition, the BMD regime includes both monotonically decreasing H_L and part of the U-shaped H_L, while the MD regime includes both monotonically increasing H_L and part of the U-shaped H_L. These results demonstrate again that the U-shaped behavior occurs during the transition between the BMD and MD regimes, supporting the underlying mechanism of such flame behavior.

As observed in the experiments, flame blowout occurs after the flame has lifted sufficiently far downstream of the nozzle and is thus minimally affected by heat loss, whereas flame liftoff and blowoff are directly influenced by it. This is reflected in the new correlation in Eq. (3), which incorporates the heat loss parameter and indicates that flame liftoff and blowoff share a common mechanism governed by buoyancy, jet momentum, and heat loss. In contrast, the best-fit

correlation for flame blowout in Eq. (4) yields a zero exponent for the heat loss parameter, indicating no dependence of flame blowout on thermal interaction with the nozzle. This aligns with the understanding that flame blowout typically occurs far downstream of the nozzle, where heat loss from the flame to the nozzle rim becomes negligible.

6. Conclusions

The behavior of laminar nonpremixed flames of N_2-diluted dimethyl-ether (DME) fuel jet in a coflow jet was experimentally investigated by varying the fuel jet velocity (U_0), fuel mole fractions ($X_{F,0}$), and temperature (T_0). Three distinct trends in liftoff height (H_L) with increasing U_0 were observed: monotonically increasing, U-shaped, and monotonically decreasing H_L. In addition, two flame extinction modes such as flame blowoff and flame blowout were identified based on the jet developing length (Z_{free}).

The flame behaviors were categorized into three distinct regimes based on the Richardson number (Ri): the momentum-driven (MD), buoyancy-momentum-driven (BMD), and buoyancy-driven (BD) regimes. The unusual monotonically decreasing H_L was found to occur exclusively within the buoyancy-momentum-driven regime, where the buoyancy effect gradually decreases with increasing U_0. Accordingly, H_L correlates well with Ri, as well as T_0/T_{ref} and $X_{F,0}$, emphasizing the importance of buoyancy. In contrast, the typical monotonically increasing H_L appeared only in the momentum-driven regime, and thus H_L is better correlated with U_0/S_L^0, T_0/T_{ref}, and $X_{F,0}$, reflecting the dominant role of jet momentum. Consequently, the U-shaped H_L behavior emerged as the flame transitioned between the buoyancy-momentum-driven and momentum-driven regimes. The stabilization mechanisms of lifted flames in each regime were analyzed by examining the flame blowout and stabilization processes over time from the perspective of stabilization dynamics, utilizing laser ignition downstream of the nozzle.

In the buoyancy-momentum-driven regime with relatively low U_0, heat loss to the nozzle rim, along with jet momentum and buoyancy, significantly influenced flame liftoff. In contrast, in the momentum-driven regime with relatively high U_0, jet momentum was the primary factor causing flame liftoff from the nozzle. Finally, the blowoff and liftoff limits of attached flames were characterized using $(\rho_F - \rho_b)/\rho_F$, U_L/S_L^0, and $(T_{ad} - T_0)/T_0$, which identified the importance of heat loss to flame liftoff.

In future work, the influence of buoyancy on flame behavior will be further investigated through numerical simulations. Complementary experiments will also be conducted to examine flame characteristics in the buoyancy-driven regime.

CRediT authorship contribution statement

Dong Jun Kim: Writing – original draft, Visualization, Investigation, Formal analysis. **Jeong Park:** Writing – review & editing, Supervision, Funding acquisition. **Suk Ho Chung:** Writing – review & editing, Supervision. **Chun Sang Yoo:** Writing – review & editing, Supervision, Project administration, Funding acquisition, Formal analysis.

Declaration of competing interest

The authors declare that they have no known competing financial interests or personal relationships that could have appeared to influence the work reported in this paper.

Acknowledgments

This work was supported by the Basic Science Program through the National Research Foundation of Korea (NRF) funded by the Ministry of Science and ICT (RS-2023-451310 and RS-2024-00356149).

Appendix A. Supplementary data

Supplementary material related to this article can be found online at https://doi.org/10.1016/j.combustflame.2025.114396.

References

[1] S.H. Chung, B.J. Lee, On the characteristics of laminar lifted flames in a nonpremixed jet, Combust. Flame 86 (1991) 62–72.
[2] B.J. Lee, S.H. Chung, Stabilization of lifted tribrachial flames in a laminar nonpremixed jet, Combust. Flame 109 (1997) 163–172.
[3] B.J. Lee, M.S. Cha, S.H. Chung, Characteristics of laminar lifted flames in a partially premixed jet, Combust. Sci. Technol. 127 (1997) 55–70.
[4] Y.S. Ko, S.H. Chung, Propagation of unsteady tribrachial flames in laminar non-premixed jets, Combust. Flame 118 (1999) 151–163.
[5] S.H. Chung, Stabilization, propagation and instability of tribrachial triple flames, Proc. Combust. Inst. 31 (2007) 877–892.
[6] Y.-C. Chen, R.W. Bilger, Stabilization mechanisms of lifted laminar flames in axisymmetric jet flows, Combust. Flame 122 (2000) 377–399.
[7] J.W. Dold, Flame propagation in a nonuniform mixture: analysis of a slowly varying triple flame, Combust. Flame 76 (1989) 71–88.
[8] P.N. Kioni, B. Rogg, K.N.C. Bray, A. Liñán, Flame spread in laminar mixing layers: the triple flame, Combust. Flame 95 (1993) 276–290.
[9] G.R. Ruetsch, L. Vervisch, A. Liñán, Effects of heat release on triple flames, Phys. Fluids 7 (1995) 1447–1454.
[10] J. Daou, A. Liñán, The role of unequal diffusivities in ignition and extinction fronts in strained mixing layers, Combust. Theory Model. 2 (1998) 449.
[11] S.H. Won, S.H. Chung, M.S. Cha, B.J. Lee, Lifted flame stabilization in developing and developed regions of coflow jets for highly diluted propane, Proc. Combust. Inst. 28 (2000) 2093–2099.
[12] S.H. Won, J. Kim, K.J. Hong, M.S. Cha, S.H. Chung, Stabilization mechanism of lifted flame edge in the near field of coflow jets for diluted methane, Proc. Combust. Inst. 30 (2005) 339–347.
[13] K. Van, K.S. Jung, C.S. Yoo, S. Oh, B.J. Lee, M.S. Cha, J. Park, S.H. Chung, Decreasing liftoff height behavior in diluted laminar lifted methane jet flames, Proc. Combust. Inst. 37 (2019) 2005–2012.
[14] K.H. Van, J. Park, S.H. Yoon, S.H. Chung, M.S. Cha, Mechanism on oscillating lifted flames in nonpremixed laminar coflow jets, Proc. Combust. Inst. 37 (2019) 1997–2004.
[15] S. Oh, K.H. Van, K.S. Jung, C.S. Yoo, M.S. Cha, S.H. Chung, J. Park, On the oscillating flame characteristics in nonpremixed laminar coflow-jets: an experimental and numerical study, Proc. Combust. Inst. 38 (2021) 2049–2056.
[16] K.H. Van, S. Oh, M.S. Cha, C.S. Yoo, J. Park, S.H. Chung, Effects of schmidt number on non-monotonic liftoff height behavior in laminar coflow-jet flames with diluted methane and ethylene, Proc. Combust. Inst. 38 (2021) 1913–1921.
[17] D.J. Kim, S.Y. Oh, C.S. Yoo, J. Park, S.H. Chung, Non-monotonic liftoff height behaviors in laminar nonpremixed coflow jet flames of dme with ambient temperature variation, Proc. Combust. Inst. 40 (2024) 105210.
[18] S. Deng, P. Zhao, M.E. Mueller, C.K. Law, Autoignition-affected stabilization of laminar nonpremixed dme/air coflow flames, Combust. Flame 162 (2015) 3437–3445.
[19] K.S. Jung, B.R. Jung, S.H. Kang, S.H. Chung, C.S. Yoo, A numerical study of the pyrolysis effect on autoignited laminar lifted dimethyl ether jet flames in heated coflow air, Combust. Flame 209 (2019) 225–238.
[20] S.M. Al-Noman, B.C. Choi, S.H. Chung, Autoignited lifted flames of dimethyl ether in heated coflow air, Combust. Flame 195 (2018) 75–83.
[21] S.R. Gollahalli, Ö. Savaş, R.F. Huang, J.L. Rodriquez Azara, Structure of attached and lifted gas jet flames in hysteresis region, Symp. (Int.) Combust. 21 (1988) 1463–1471.
[22] J. Lee, S.H. Chung, Characteristics of reattachment and blowout of laminar lifted flames in partially premixed propane jets, Combust. Flame 127 (2001) 2194–2204.
[23] ANSYS Inc., Chemkin-pro, version 2022 r2, 2014, Available at http://www.reactiondesign.com.
[24] R.J. Kee, J.F. Grcar, M.D. Smooke, J.A. Miller, E. Meeks, PREMIX: a FORTRAN Program for Modeling Steady Laminar One-Dimensional Premixed Flames, Tech. Rep. SAND85-8249, Sandia National Labs, Livermore, CA, USA, 1985.
[25] Z. Zhao, M. Chaos, A. Kazakov, F.L. Dryer, Thermal decomposition reaction and a comprehensive kinetic model of dimethyl ether, Int. J. Chem. Kinet. 40 (2008) 1–18.
[26] M.A. Delichatsios, Transition from momentum to buoyancy-controlled turbulent jet diffusion flames and flame height relationships, Combust. Flame 92 (1993) 349–364.

[27] D. Li, Y. Wen, Y.C. Liu, S. Wang, On the transition modes and mechanisms for laminar to turbulent lifted jet diffusion flames at normal- and micro-gravity, Combust. Flame 260 (2024) 113269.
[28] C.K. Law, Combustion Physics, Cambridge University Press, 2006.
[29] V.N. Kurdyumov, M. Matalon, The porous-plug burner: flame stabilization, onset of oscillation, and restabilization, Combust. Flame 153 (2008) 105–118.
[30] A. Stagni, Y. Luo, M. Steinhausen, A. Dreizler, C. Hasse, Chemistry effects in the wall quenching of laminar premixed dme flames, Combust. Flame 232 (2021) 111529.
[31] A. Fan, K. Maruta, H. Nakamura, S. Kumar, W. Liu, Experimental investigation on flame pattern formations of dme–air mixtures in a radial microchannel, Combust. Flame 157 (2010) 1637–1642.